Case Studies in Thermal Engineering 45 (2023) 102948

Contents lists available at ScienceDirect

Case Studies in Thermal Engineering

journal homepage: www.elsevier.com/locate/csite

New fractional approach for the simulation of (Ag) and (TiO_2) mixed hybrid nanofluid flowing through a channel: Fractal fractional derivative

Kehong Zheng [a], Ali Raza [b,c], Ahmed M. Abed [d,e], Hina Khursheed [b], Laila F. Seddek [f,g], Ali Hasan Ali [h,i,*], Absar Ul Haq [j]

[a] College of the Water Conservancy and Ecological Engineering, Nanchang Institute of Technology, Nanchang, 330099, China
[b] Department of Mathematics, Minhaj University Lahore, Pakistan
[c] Department of the Mathematics, University of Engineering and Technology Lahore, Pakistan
[d] Department of the Industrial Engineering, College of Engineering, Prince Sattam Bin Abdulaziz University, Al Kharj, 16273, Saudi Arabia
[e] Industrial Engineering Department, Zagazig University, Zagazig, 44519, Egypt
[f] Department of the Mathematics, College of Science and Humanities in Al-Kharj, Prince Sattam bin Abdulaziz University, Al-Kharj, P.O. Box 11942, Saudi Arabia
[g] Department of the Engineering Mathematics and Physics, Faculty of Engineering, Zagazig University, Zagazig, 44519, Egypt
[h] Institute of the Mathematics, University of Debrecen, Pf. 400, H-4002, Debrecen, Hungary
[i] Department of Mathematics, College of Education for Pure Sciences, University of Basrah, Basrah, 61001, Iraq
[j] Department of the Mathematics, University of Engineering and Technology Lahore (Narowal Campus), Pakistan

ARTICLE INFO

Keywords:
Fractal-fractional derivatives
Water
Hybrid-nanofluid
Parallel plates
Laplace transform

ABSTRACT

This paper presents a novel application of the Fractal Fractional derivative to control the flow of non-Newtonian fluids. The study focuses on the generalized magnetohydrodynamic (MHD) flow of a Casson-type hybrid nanofluid in a micro-channel and its modeling and solution. The hybrid nanofluid mixed with the suspension of copper (Cu) and titanium dioxide (TiO_2) nanoparticles with carboxymethyl cellulose (CMC) and water (H_2O) as base fluids are considered. First, the partial differential equations are converted to a fractional model with the current and new description of fractional derivatives, i.e., Fractal fractional derivatives. Then, ordinary differential equations are resolved numerically using a fractional Laplace transformation. Finally, the results are numerically calculated and shown in various graphs with a physical description to study the physical importance of different relevant factors. As a result, it's computed that the momentum field indicates the decaying behavior with incrementing the Casson fluid parameter. Furthermore, the impact of CMC-based hybrid nanofluid ($CMC + Ag + TiO_2$) on energy and momentum is slightly more significant than the water-based ($H_2O + Ag + TiO_2$) hybrid nanofluid. Moreover, due to the impact of volume fraction, the fluid temperature increases while velocity slows down due to increased thermal conductivity.

* Corresponding author. Institute of the Mathematics, University of Debrecen, Pf. 400, H-4002, Debrecen, Hungary.
E-mail addresses: yyymath@126.com (K. Zheng), aliraza.math@mul.edu.pk (A. Raza), a.abed@psau.edu.sa (A.M. Abed), hina.math@mul.edu.pk (H. Khursheed), l.morad@psau.edu.sa (L.F. Seddek), ali.hasan@science.unideb.hu (A.H. Ali), absarulhaq@uet.edu.pk (A.U. Haq).

https://doi.org/10.1016/j.csite.2023.102948
Received 8 February 2023; Received in revised form 17 March 2023; Accepted 25 March 2023
Available online 30 March 2023

Nomenclature

θ	Angle of magnetic inclination (−)
T_d	Ambient temperature (K)
U_0	Characteristic velocity (ms^{-1})
μ_{nf}	Dynamic viscosity (Kg/ms)
σ	Electrical Conductivity (−)
U_1	Fluid velocity (m/s)
α, β	Fractional parameters (−)
g	Gravity acceleration (m/s^2)
Gr	Heat Grashof number (−)
q	Laplace transform variable (−)
Gm	Mass Grashof number (−)
M	Magnetic field (−)
Nu	Nusselt number (−)
ρ_{nf}	Nano-fluid density (Kg/m^3)
Pr_{eff}	Prandtl number (−)
C_p	Specific heat at the constant pressure (J/kgK)
C_f	Skin friction (−)
Sh	Sherwood number (−)
Sh	Sherwood number (−)
Sc	Schmidt number (−)
B_o	Strength of Magnetic field (Kg/s^2)
τ	Times (s)
β_T	Thermal expansion coefficient ($1/k$)
k_{nf}	Thermal Conductivity of the Nanofluid (W/mk)
T_w	Wall temperature (K)

1. Introduction

Despite extensive study on nanofluids, integer-order partial differential equations cannot account for the memory effect. The fractionalized nanofluids simulations are extra thorough and more effective at shedding light on how the memory effect and flow parameters interact. Numerous scientific phenomena, such as viscoelastic materials, electromagnetic theory, fluid flow, diffusive transport, electrical networks, etc., can be described using non-integer order derivatives [1–4]. The elliptic decay function and generalized Mittag-Leffler are the three fundamental arithmetic functions that numerous corporal and real-world events adhere to Ref. [5]. Recent literature shows that many fractional operators have mathematical formulations depending on these functions. The RL-fractional and CF-derivative are two examples of fractional derivatives that lie on power law kernels. For a long time, the RLFD and CFD have been effectively applied to various issues in real-world settings [6]. The singular is the basis of CFD. However, in RLFD, the derivative of a constant is not 0. The limitations of the RLFD and CFD are overcome by the CF-fractional derivative, which lies on the exponential kernel. Recent developments in RL and CF derivatives were familiarized by Atangana and Baleanu [7]. The generalized Mittag-Leffler function, free of singularity and localization, is the foundation for the AB-fractional derivative (ABFD) kernel. It is okay to use ABFD to describe the actual physical events. The non-singularity and without locality of the based kernel are the properties that best explain the memory inside the structure with varied scales. The AB operators also adhere to all formal specifications for fractional calculus [8–11].

Researchers from a range of disciplines and specialties are interested in the phenomenon of heat transmission. In fluid dynamics, convection heat transfer is significant. Several techniques can be used to speed up the heat transfer rate in order to reach the needed thermal efficiency. Maxwell was the first to suggest using nanoparticles to accelerate the heat transmission rate, a groundbreaking publication. Choi increased thermal conductivity and heat transmission rate using nanoparticles [12]. Here are some fascinating recent theoretical studies on nanofluids. Although nanofluids have been employed in industry on a practical basis, a competitive fluid must still attain the required thermal efficiency. By floating various types of nanoparticles in the working fluid, so-called hybrid nanofluids, an improved type of nanofluid with more excellent thermal conductivity, have been discovered [13]. However, hybrid nanoparticles have received microscopic investigation, and more has to be done in this field. Han et al. [14] created a sophisticated sort of nanoparticle that included an alumina/iron oxide sphere and a hybrid CNT particle. There was a 21% increase in heat conductivity. Nine et al. [15] examined the thermal rise caused by the dispersion of Cu2O and Cu/Cu2O. According to Sarkar et al. [16] examination of hybrid nanofluids, actual hybridization can aid in creating more thermally efficient nanofluids.

Fractional calculus is a valuable tool for describing challenging and real-world problems related to rheology, fluid flow, diffusive transport, and electromagnetic theory, according to several recent research [17–19]. The power function, the modified Mittag-Leffler

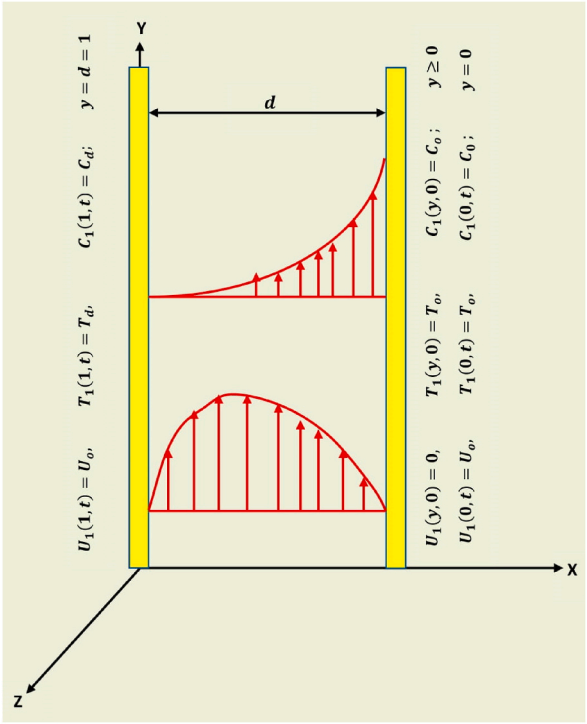

Fig. 1. Flow geometry.

function, and the elliptic decay function are three critical mathematical ideas that support real-world problems [20]. Which fractional operator is most appropriate for describing complex and real-world problems is currently up for debate. Some realistic mathematicians believe that the Caputo fractional operator, which permits the typical initial circumstances in the presentation of integral transform, is a valuable tool for defining such scenarios [21]. The foundation of this defense is the researchers' desire to accept the fractional operator as ordinary. However, other academics concur that the RL operator is superior since it allows for deriving the initial conditions with a fractional kernal, which is more realistic when employing the Laplace transform [22].

Atangana has looked at how fractal and fractional derivatives are related in order to compute the problems in real-world scenarios [23]. In the year prior, Atangana et al. [24] and Atangana et al. [25] presented a complete evaluation of recently presented operators to solve fractal fractional differential equations. Mathematical and numerical analysis of a multi-dimensional chaotic system without an equilibrium position in a fractal-fractional Mittag-Leffler kernel is presented in Ref. [26]. A collection of the fractional-order system of equations with singularity and strong nonlinear effects relevant to electrodynamics flow in a circular cylindrical conduit has numerical methods found by Srivastava et al. [27]. The scientific fractional Casson fluid model, characterized by the Constant Proportional Caputo fractional constraint having a non-local and singular kernel over an infinitely vertical surface, was investigated analytically by Rehman et al. [28] using a fractional fractal approach. In order to understand the origin or flow of viscous fluid, Imran recently investigated the fractal fractional derivative. The flow between two infinitely long parallel plates is being affected by MHD. However, the unique idea of the fractal-fractional derivative has not yet been put into practice to study the heat transfer problem with fluid flow. Thus, using the unique fractal-fractional derivative technique, we represent the first work to address a heat transfer issue connected to fluid motion.

Physical boundary conditions are considered along with heat transfer and free convection movement. Since the parallel plates are fixed, and the fluid passes through the appropriate channels, convection heating from the parallel plates generates motion. No studies have yet used the novel concept of fractal-fractional derivatives with the power-law kernel. The Laplace method is used to identify the issue's solution. Mathcad-15 explores the effects of fractal and fractional parameters on temperature and velocity. The authors [29] found that no researchers had looked at the Couttee flow Casson fluid model using the fractional fractal model of exponential memory in light of the prior literature. Memory and fractal behavior are considered via a fractal-fractional differential operator, which is only conceivable with fractal-fractional derivatives. As a result, a modest amount of specialized literature exists on power law memory. However, no one has ever looked into the fractal-fractional analysis of exponential memory for Casson fluid or any other fluid type. The employed numerical method is efficient and robust and can produce convergent and stable findings for any mesh or step size. This tactic converges faster than other explicit methods now employed to address similar problems since it is implicit. The fractal-fractional mathematical models for the helium burning system have a numerical solution established by Shloof et al. [30]. According to Abro et al. [31], the embedded rheological parameters have shown several similarities and contrasts in power law-based new velocity field behavior in fractal-fractionalized Ferro-fluid. No previous studies on ferrofluid have utilized a fractal-fractional derivative based on the power law must be emphasized. More recent studies on the definition of fractional derivatives can be found in Refs. [26,32–36].

This article discusses applying the fractal-fractional concept of non-Newtonian viscose fluid between concurrent infinite plates. This study uses hybrid nanofluids based on CMC and H_2O to study free convection flows with fractionalized heat transfer over a vertical channel. Generalized non-integer governed equations for thermal transmission serve as the foundation for this mathematical model. In this paper, we developed a fractional model based on a time-fractional Fractal operator to account for generalized memory effects. The Laplace system is used to get answers to the dimensionless temperature, concentration, and temperature. The accuracy of the generated solutions is evaluated using tabular analysis. For Laplace inversion, Tzou and Stehfest's numerical methods were used. Finally, the effects of various constraints on various nanoparticles are assessed on a visual plot.

2. Problem description

Let's investigate the MHD flow of a generalized Casson-type hybrid nanofluid in a vertical micro-channel. Two similar plates are situated at a distance, d apart, to form the channel. While the y-axis is set at right angles to the flow direction, the fluid flows in the x-direction. The fluid is not moving, and the plate's temperature at $y = 0$ equals T_o, at the instant when $t = 0$. By increasing the temperature of the plate at $y = L$ from T_o to T_w after $T > 0^+$, the buoyancy force is increased. The Casson fluid constitutive model is provided, and Fig. 1 depicts the physical configuration. A uniform inclined magnetic field controls the incompressible Casson hybrid nanofluid flow, a porous material, and heat transfer. For this flow model, the following assumptions are made.

- The length of parallel plates is infinite with width d.
- The pour plates are aligned in the x direction and are perpendicular to the y axis.
- At $t \leq 0$, both temperature and concentration have persistent values as T_d and C_d respectively.
- Different nanoparticle mixed hybrid-nanofluid accelerates in the x-direction.
- The constant strength magnetic field B_o is pragmatic to flowing fluid.

By utilizing the Boussinseq's approximation [37] and Roseland approximations [38], It is possible to formulate the guided partial differential equations as follows [20].

$$\rho_{hnf}\frac{\partial U_1(y,t)}{\partial t} = \mu_{hnf}\left(1+\frac{1}{\lambda}\right)\frac{\partial^2 U_1(y,t)}{\partial y^2} - \sigma_{hnf}B_o^2\, sin(\theta)U_1(y,t) - \left(1+\frac{1}{\lambda}\right)\frac{\varphi_{hnf}}{k}U_1(y,t) + g(\rho\beta_T)_{hnf}(T_1(y,t)-T_0) + g(\rho\beta_T)_{hnf}(C_1(y,t)-C_0) \tag{1}$$

$$\left(\rho C_p\right)_{hnf}\frac{\partial T_1(y,t)}{\partial t} = \frac{\partial^2 T_1(y,t)}{\partial y^2} \tag{2}$$

$$\frac{\partial C_1(y,t)}{\partial t} = D\frac{\partial^2 C_1(y,t)}{\partial y^2} \tag{3}$$

where the nomenclature section contains a list of all the requirements and variables. The constant conditions for temperature, concentration, and momentum equations are as follows

$$U_1(y,0) = 0, T_1(y,0) = T_o, C_1(y,0) = C_o \tag{4}$$

$$U_1(0,t) = 0, T_1(0,t) = T_o, C_1(0,t) = C_o \tag{5}$$

$$U_1(L,t) = U_w, T_1(L,t) = T_w, C_1(L,t) = C_w \tag{6}$$

The connected governed equations may not be examined with the dimension of the impact of all process variables now that the subsequent dimensionless variables have been incorporated.

$$U_1^* = \frac{d}{\nu_f}U_1, t^* = \frac{\nu t}{L^2}, y^* = \frac{y}{L}, T_1^* = \frac{T_1(y,t)-T_o}{T_w-T_o}, C_1^* = \frac{C_1(y,t)-C_o}{C_w-C_o}$$

$$Sc = \frac{\nu}{D}, M = \frac{\sigma_f L^2 B_o^2}{\mu_f}, Gr = \frac{g\beta_T L^3(T_w-T_o)}{\nu^2}, K_{eff} = \frac{\nu\,\varphi}{K^* U_o^2}, Pr = \frac{\mu_f C_p}{k_f},$$

$$\lambda_{hnf} = \frac{k_{hnf}}{k_f}, Gm = \frac{g\beta_C(N_w-N_o)L^3}{\nu^2}, \lambda_1 = \frac{\lambda}{\lambda+1}$$

Utilizing the above none-dimensional restraints in the leading equations and conditions (1)–(6), one can obtain by adjusting the above-mentioned dimensionless variables while ignoring the 〃∗〃 symbols

$$\frac{\partial U_1(y,t)}{\partial t} = \frac{1}{\lambda_1}\frac{\partial^2 U_1(y,t)}{\partial y^2} - \left(Msin(\theta)+K_{eff}\right)U_1(y,t) + GrT_1(y,t) + GmC_1(y,t) \tag{7}$$

Table 1
The magnitudes of hybrid-nanofluids thermo-physical properties.

Quantities	Nanofluid	Hybrid Nanofluid
Density	$\rho_{nf} = (1-\varphi)\rho_f + \varphi\rho_s$	$\rho_{hnf} = (1-\varphi_{hnf})\rho_f + \varphi_{Tio_2}\rho_{Tio_2} + \varphi_{Ag}\rho_{Ag}$
Dynamic Viscosity	$\mu_{nf} = \mu_f/(1-\varphi)^{5/2}$	$\mu_{hnf} = \mu_f/[1-(\varphi_{Ag}+\varphi_{Tio_2})]^{5/2}$
Electrical conductivity	$\sigma_{nf}/\sigma_f = 1+3(\sigma_s/\sigma_f - 1)\varphi/(\sigma_s/\sigma_f + 2) - (\sigma_s/\sigma_f - 1)\varphi$	$\sigma_{hnf}/\sigma_f = 1+3(\varphi_{Ag}\sigma_{Ag} + \varphi_{Tio_2}\sigma_{Tio_2}/\sigma_f - \varphi_{hnf})/\varphi_{Ag}\sigma_{Ag} + \varphi_{Tio_2}\sigma_{Tio_2}/\varphi_{hnf}\sigma_f + 2 - (\varphi_{Ag}\sigma_{Ag} + \varphi_{Tio_2}\sigma_{Tio_2}/\sigma_f - \varphi_{hnf})$
Thermal conductivity	$K_{nf}/K_f = k_s + 2k_f - 2\varphi(k_s - k_f)/k_s + 2k_f + \varphi(k_s - k_f)$	$K_{hnf}/K_f = \varphi_{Ag}k_{Ag} + \varphi_{Tio_2}k_{Tio_2}/ - \varphi_{hnf} + 2k_f + 2(\varphi_{Ag}k_{Ag} + \varphi_{Tio_2}k_{Tio_2}) - 2\varphi_{hnf}K_f/\varphi_{Ag}k_{Ag} + \varphi_{Tio_2}k_{Tio_2}/\varphi_{hnf} + 2k_f + (\varphi_{Ag}k_{Ag} + \varphi_{Tio_2}k_{Tio_2}) - \varphi_{hnf}K_f$
Heat capacitance	$(\rho C_p)_{nf} = (1-\varphi)(\rho C_p)_f + \varphi(\rho C_p)_s$	$(\rho C_p)_{hnf} = (1-\varphi_{hnf})(\rho C_p)_f + \varphi_{Ag}(\rho C_p)_{Ag+}\varphi_{Tio_2}(\rho C_p)_{Tio_2}$
Thermal Expansion Coefficient	$(\rho B_T)_{nf} = (1-\varphi)(\rho B_T)_f + \varphi(\rho B_T)_s$	$(\rho B_T)_{hnf} = (1-\varphi_{hnf})(\rho B_T)_f + \varphi_{Ag}(\rho B_T)_{Ag} + \varphi_{Tio_2}(\rho B_T)_{Tio_2}$

Table 2
The Nanoparticles' and normal fluids' thermal properties.

Material	*CMC*	H_2O	TiO_2	*Ag*
$\boldsymbol{\rho(kg/m^3)}$	997	997.1	425	10500
$\boldsymbol{C_p(J/kg\,K)}$	4179	4179	6862	235
$\boldsymbol{k(W/m\,K)}$	0.613	0.613	8.9538	429
$\boldsymbol{\beta_T \times 10^{-5}(K^{-1})}$	0.9	21	0.9	1.89
$\boldsymbol{\sigma}$	0.04	0.05	1×10^{-12}	3.6×10^{7}

$$Pr_{eff}\frac{\partial T_1(y,t)}{\partial t} = \frac{\partial^2 T_1(y,t)}{\partial y^2} \tag{8}$$

$$Sc\frac{\partial C_1(y,t)}{\partial t} = \frac{\partial^2 C_1(y,t)}{\partial y^2} \tag{9}$$

With the consistent dimensionless conditions

$$U_1(y,0) = 0, T_1(y,0) = 0, C_1(y,0) = 0 \tag{10}$$

$$U_1(0,t) = 0, T_1(0,t) = 0, C_1(0,t) = 0 \tag{11}$$

$$U_1(L,t) = 1, T_1(L,t) = 1, C_1(L,t) = 1 \tag{12}$$

where $M, K_{eff}, \lambda_1, Gr, Gm$ respectively, stand in for the applied magnetic field constraint, effective porosity, Casson fluid parameter, heat, and mass transfer. Tables 1 and 2 lists the thermal properties of the base material, the solid nanoparticles, and the hybrid nanofluid model.

3. Basic definitions

Assuming that $y(x)$ is a continuous function, the non-integer derivative of y of order (β) in the RL form with power, the law can be expressed as

$${}^{FFP}\mathfrak{D}_x^{\alpha,\beta}y(x) = \frac{1}{\Gamma(1-\alpha)}\frac{d}{dx^\beta}\int_0^x y(t)(x-t)^{-\alpha}dt, 0<\alpha,\beta\le 1$$

$$\frac{dy(t)}{dx^\beta} = \lim_{x\to t}\frac{y(x)-y(t)}{x^\beta - t^\beta} \tag{13}$$

Usual Laplace Transformation: Let's define $y(x)$ for instance where $(x>0)$. The LT of $y(x)$ is a non-fractional transform provided by the Laplace integral and is well-defined as $Y(s)$ or $\mathscr{L}\{y(x)\}$.

$$\mathscr{L}\{y(x)\} = Y(x) = \int_0^\infty exp(-sx)f(x)dx \tag{14}$$

Fractal Laplace Transformation: Suppose a continuous function $g(x)$, then its fractal-Laplace can be described as [32]

$${}^{F}\mathscr{L}_p^{\alpha}\{g(x)\} = G(x) = \int_0^\infty exp(-sx)x^{\alpha-1}g(x)dx \tag{15}$$

As by the above equation for $\alpha\to1$ the usual Laplace can be attained.

Table 3
Numerical impact of numerical approaches.

y	$T_1(y,t)$ with Stehfest	$T_1(y,t)$ with Tzou's	$C_1(y,t)$ with Stehfest	$C_1(y,t)$ with Tzou's	$U_1(y,t)$ with Stehfest	$U_1(y,t)$ with Tzou's
0.1	0.0169	0.0409	0.0759	0.0770	0.1089	0.1090
0.2	0.1419	0.2013	0.1534	0.1554	0.2121	0.2122
0.3	0.3940	0.4570	0.2338	0.2367	0.3036	0.3036
0.4	0.6117	0.6429	0.3184	0.3223	0.3770	0.3770
0.5	0.7486	0.7724	0.4096	0.4137	0.4256	0.4256
0.6	0.8617	0.8683	0.5082	0.5124	0.4418	0.4419
0.7	0.8941	0.9020	0.6158	0.6198	0.4174	0.4174
0.8	0.9662	0.9641	0.7337	0.7369	0.3428	0.3429
0.9	0.9907	0.9959	0.8623	0.8641	0.2077	0.2077

Table 4
Numerical analysis of Nusselt number and Skin friction at different time.

α,β	Nu at $t = 0.5$	Nu at $t = 1.0$	Sh at $t = 0.5$	Sh at $t = 1.0$	C_f at $t = 0.5$	C_f at $t = 1.0$
0.1	0.5749	0.5836	0.3864	0.3913	0.4439	0.4461
0.2	0.5449	0.5623	0.3686	0.3791	0.4370	0.4475
0.3	0.5159	0.5412	0.3513	0.3665	0.4325	0.4475
0.4	0.4886	0.5207	0.3364	0.3542	0.4286	0.4468
0.5	0.4631	0.5011	0.3187	0.3422	0.4247	0.4456
0.6	0.4392	0.4823	0.3035	0.3307	0.4206	0.4444
0.7	0.4171	0.4643	0.2891	0.3195	0.4163	0.4431
0.8	0.3964	0.4472	0.2754	0.3087	0.4117	0.4418
0.9	0.3773	0.4310	0.2624	0.2982	0.4068	0.4406

4. Solution of the governed equations

The Fractal fractional model for the governed problem can be implemented as

$$ {}^{C}\mathfrak{D}_t^{\alpha} U_1(y,t) = \beta t^{\beta-1}\left\{\frac{1}{\lambda_1}\frac{\partial^2 U_1(y,t)}{\partial y^2} - \left(Msin(\theta)+K_{eff}\right)U_1(y,t) + GrT_1(y,t) + GmC_1(y,t)\right\} - \frac{U_1(y,0)}{\Gamma(1-\alpha)}t^{-\alpha} \tag{16} $$

$$ {}^{C}\mathfrak{D}_t^{\alpha} T_1(y,t) = \beta t^{\beta-1}\left\{\frac{1}{Pr_{eff}}\frac{\partial^2 T_1(y,t)}{\partial y^2}\right\} - \frac{T_1(y,0)}{\Gamma(1-\alpha)}t^{-\alpha} \tag{17} $$

$$ {}^{C}\mathfrak{D}_t^{\alpha} C_1(y,t) = \beta t^{\beta-1}\left\{\frac{1}{Sc}\frac{\partial^2 C_1(y,t)}{\partial y^2}\right\} - \frac{C_1(y,0)}{\Gamma(1-\alpha)}t^{-\alpha} \tag{18} $$

4.1. Solution of energy equation

The following results from implementing fractional LT to Eq. (15) employing Eq. (16) and operating conditions from (13), we produce the thermal solution as

$$ q^{\alpha}\overline{T}_1(y,q) - \overline{T}_1(y,0) = \beta\,\Gamma(\beta)\,q^{-\beta}\left\{\frac{1}{Pr_{eff}}\frac{\partial^2\overline{T}_1(y,q)}{\partial y^2}\right\} - \frac{\overline{T}_1(y,0)}{\Gamma(1-\alpha)}q^{-\alpha}\Gamma(1-\alpha) $$

With

$$ \overline{T}_1(1,q) = \frac{1}{q}, \overline{T}_1(0,q) = 0 $$

Utilizing the above conditions, the energy solution will be

$$ \overline{T}_1(y,q) = \frac{1}{q}\,\frac{Sinh\left[y\sqrt{\Lambda_o\,Pr_{eff}\,q^{\alpha+\beta}}\right]}{Sinh\left[\sqrt{\Lambda_o\,Pr_{eff}\,q^{\alpha+\beta}}\right]} \tag{19} $$

The Laplace inverse of energy solution will be attained in Tables 3 and 4 with different numerical approaches.

4.2. Solution of concentration profile

Employing the Laplace transform on Eq. (18) for the concentration field

$$ q^{\alpha}\overline{C}_1(y,q) - \overline{C}_1(y,0) = \beta\,\Gamma(\beta)\,q^{-\beta}\left\{\frac{1}{Sc}\frac{\partial^2\overline{C}_1(y,q)}{\partial y^2}\right\} - \frac{\overline{C}_1(y,0)}{\Gamma(1-\alpha)}q^{-\alpha}\Gamma(1-\alpha) \tag{20} $$

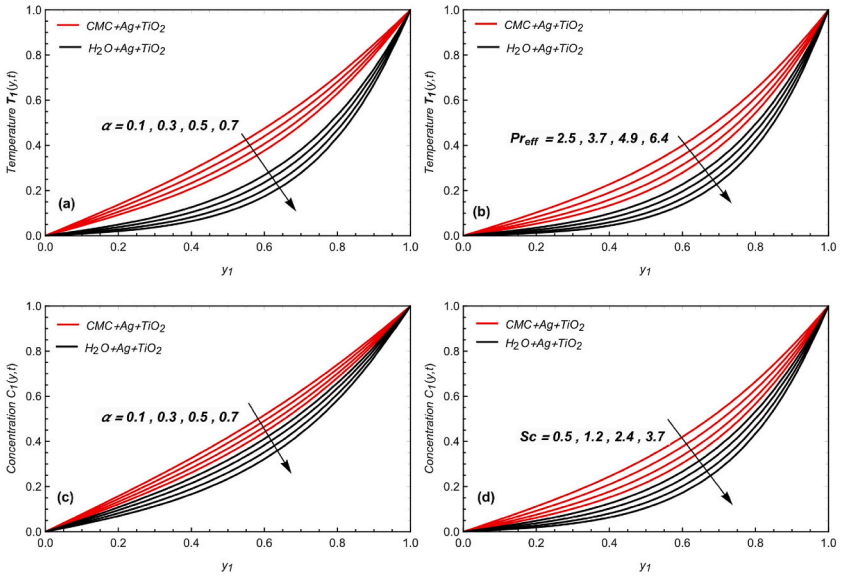

Fig. 2. $T_1(y,t)$ and $C_1(y,t)$ due to influence of different constraints.

With conditions

$$\overline{C}_1(1,q)=\frac{1}{q},\overline{C}_1(0,q)=0$$

The concentration profile, by employing the above conditions, we get

$$\overline{C}_1(y,q)=\frac{1}{q}\frac{Sinh\left[y\sqrt{\Lambda_o Sc\ q^{\alpha+\beta}}\right]}{Sinh\left[\sqrt{\Lambda_o Sc\ q^{\alpha+\beta}}\right]} \tag{21}$$

4.3. Solution of momentum field

For the momentum field, utilizing the attained results of energy and concentration fields and employing the LT on Eq. (16)

$$q^{\alpha}\overline{U}_1(y,q)-\overline{U}_1(y,0)=\beta\,\Gamma(\beta)\,q^{-\beta}\left\{\frac{1}{\lambda_1}\frac{\partial^2\overline{U}_1(y,q)}{\partial y^2}-\left(Msin(\theta)+K_{eff}\right)\overline{U}_1(y,q)+Gr\overline{T}_1(y,q)+Gm\overline{C}_1(y,q)\right\}-\frac{\overline{U}_1(y,0)}{\Gamma(1-\alpha)}q^{-\alpha}\Gamma(1-\alpha) \tag{22}$$

With

$$\overline{U}_1(1,q)=\frac{1}{q}\ \text{and}\ \overline{U}_1(0,q)=0$$

So

$$\begin{aligned}\overline{U}_1(y,q)=&\left(\frac{\lambda_1\,Gr}{q}\,\frac{1}{\left(\Lambda_o\,Pr_{eff}\,q^{\alpha+\beta}\right)-\lambda_1\left(M\,sin(\theta)+K_{eff}+\Lambda_o q^{\alpha+\beta}\right)}+\frac{\lambda_1\,Gm}{q}\,\frac{1}{\left(\Lambda_o\,Sc\,q^{\alpha+\beta}\right)-\lambda_1\left(Msin(\theta)+K_{eff}+\Lambda_o q^{\alpha+\beta}\right)}\right)\\&\frac{Sinh\left(y\sqrt{\lambda_1\left(Msin(\theta)+K_{eff}+\Lambda_o q^{\alpha+\beta}\right)}\right)}{Sinh\left(\sqrt{\lambda_1\left(Msin(\theta)+K_{eff}+\Lambda_o q^{\alpha+\beta}\right)}\right)}+\frac{1}{q}\,\frac{Sinh\left(y\sqrt{\lambda_1\left(Msin(\theta)+K_{eff}+\Lambda_o q^{\alpha+\beta}\right)}\right)}{Sinh\left(\sqrt{\lambda_1\left(Msin(\theta)+K_{eff}+\Lambda_o q^{\alpha+\beta}\right)}\right)}-\frac{\lambda_1\,Gr}{q}\\&\frac{1}{\left(\Lambda_o\,Pr_{eff}\,q^{\alpha+\beta}\right)-\lambda_1\left(Msin(\theta)+K_{eff}+\Lambda_o q^{\alpha+\beta}\right)}\,\frac{Sinh\left(y\sqrt{\left(\Lambda_o\,Pr_{eff}\,q^{\alpha+\beta}\right)}\right)}{Sinh\left(\sqrt{\left(\Lambda_o\,Pr_{eff}\,q^{\alpha+\beta}\right)}\right)}\\&-\frac{\lambda_1\,Gm}{q}\,\frac{1}{\left(\Lambda_o\,Sc\,q^{\alpha+\beta}\right)-\lambda_1\left(Msin(\theta)+K_{eff}+\Lambda_o q^{\alpha+\beta}\right)}\,\frac{Sinh\left(y\sqrt{\left(\Lambda_o\,Sc\,q^{\alpha+\beta}\right)}\right)}{Sinh\left(\sqrt{\left(\Lambda_o\,Sc\,q^{\alpha+\beta}\right)}\right)}\end{aligned} \tag{20}$$

Analyzing the momentum, concentration, and temperature profile results is problematic. As numerous authors have done, we also employed numerical approaches for the Laplace inverse, namely Stehfest and Tzou's numerical schemes. The precise formulations of these algorithms [4,39,40] can be characterized as

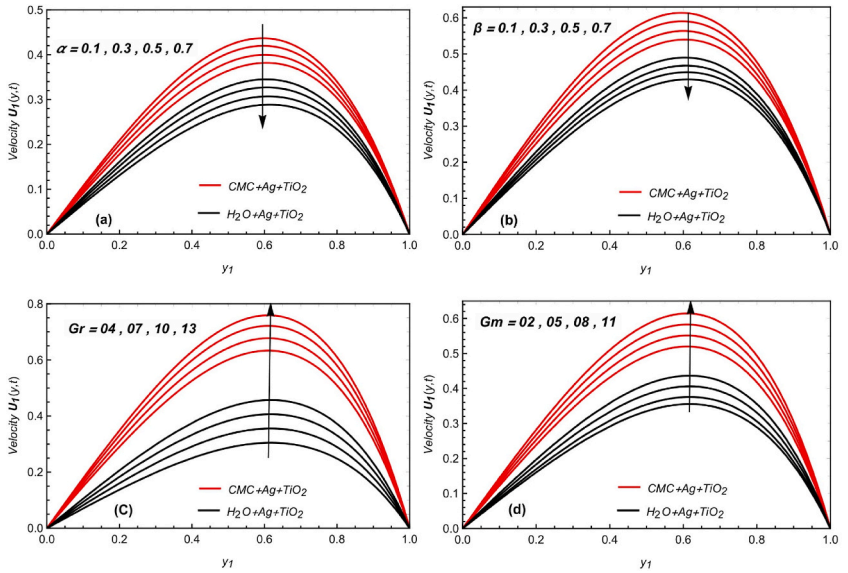

Fig. 3. $U_1(y,t)$ due to the influence of **(a):** α **(b):** β **(c):** Gr **(d):** Gm with $\varphi = 0.02, M = 2.5, Pr_{eff} = 6.3, Sc = 2.5, \lambda_1 = 1.5, \theta = \pi/4, t = 1.0$.

$$U_1(y,\tau) = \frac{ln(2)}{\tau}\sum_{i=1}^{N} v_i \overline{U_1}\left(y, i\frac{ln(2)}{\tau}\right)$$

$$v_i = (-1)^{i+\frac{N}{2}} \sum_{m=\left[\frac{q+1}{2}\right]}^{min\left(q,\frac{N}{2}\right)} \frac{m^{\frac{N}{2}}(2m)!}{\left(\frac{N}{2}-m\right)!m!\,(m-1)!\,(q-m)!\,(2m-q)!}$$

and

$$U_1(y,\tau) = \frac{e^{4.7}}{\tau}\left[\frac{1}{2}\overline{U}\left(m,\frac{4.7}{\tau}\right) + Re\left\{\sum_{j=1}^{N}(-1)^k \overline{U_1}\left(m,\frac{4.7+k\pi i}{\tau}\right)\right\}\right]$$

5. Discussion of results

The physical possessions of the several relevant constraints on the distributions of velocity, concentration, and temperature are covered in this section. A new description of fractal fractional derivatives is applied to the flowing MHD (Magnetohydrodynamics) hybrid nanofluid mixed with diverse (Ag, TiO_2) nanoparticles and with (CMC, H_2O) as base fluids. Figures display the velocity distribution data. Additionally, a tabular comparison of the temperature and velocity data is performed. The physical boundary conditions are used to build the fractal-fractional model. The problem is solved using the fractal Laplace transform method during the dimensionless analysis to get the precise solution. Finally, it examines, using graphical representation, the effects of fractal and fractional operators on various profiles.

To investigate the effect of α, Pr_{eff} on the temperature profile, Fig. 2(a and b) are conspired. The temperature distribution is seen to shrink as the fractal-fractional parameter and Prandtl number is increased. The memory phenomenon, which regulates fluid velocity and the temperature field, is improved by increased fractional constraints. Due to its most modified mathematical kernel, the memory impact is more improved for Fractal fractional derivative operator than other fractional derivative definitions. Additionally, as Pr_{eff} rises, the heat transmission rate is restricted as the material's thermal diffusivity declines. Additionally, due to the physical relevance of the considered nanoparticles, the thermal profile has a more significant impact on the (CMC) hybrid nanofluid than the (H_2O) based hybrid nanofluid when comparing the various considered hybrid nanofluids. Plots of Fig. 2(c and d) show the impact of α, Sc on the concentration profile. It demonstrates that the concentration profile declines as the fractional parameter and Schmidt number are raised. The fluctuation in fractional constraints illustrates the memory impact of focus over time. Due to both constraints, the concentration field can be controlled by raising its values. The modification of the different types of nanoparticles in nanofluid thin films over stretched layers has an impact on temperature and concentration profiles. Due to the base fluid's enhanced thermal conductivity and fractal-fractional parameter, nanoparticles cause the base fluid to become hotter. Again like the thermal field, the concentration field for the $(H_2O - Ag - TiO_2)$ based flowing fluid is lesser than the $(CMC - Ag - TiO_2)$ based hybrid nanofluid.

Fig. 3(a and b) are designed to learn the impact of α, β on the velocity profile. These numbers definitely demonstrate the substantial

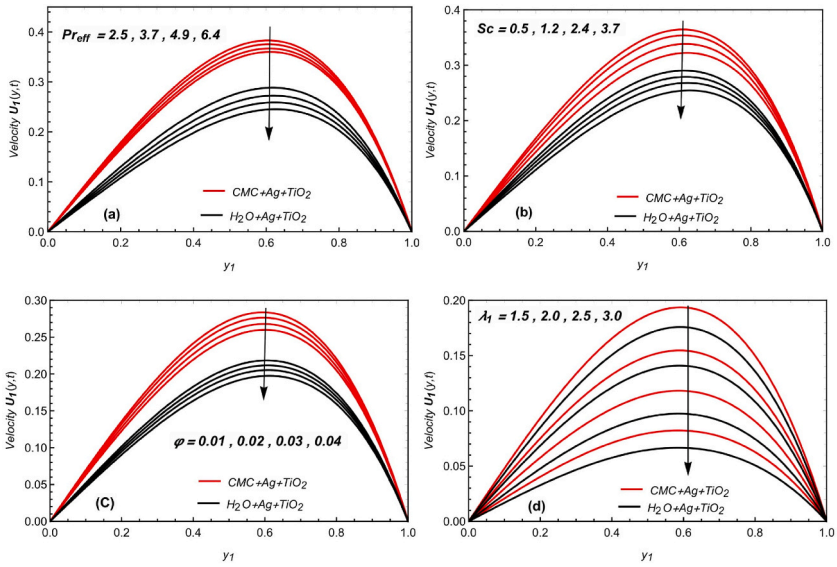

Fig. 4. $U_1(y,t)$ due to the influence of **(a):** Pr_{eff} **(b):** Sc **(c):** φ **(d):** λ_1 with $\alpha = \beta = 0.5, M = 2.5, Gr = 8.5, Gm = 7.5, \theta = \pi/4, t = 1.0$.

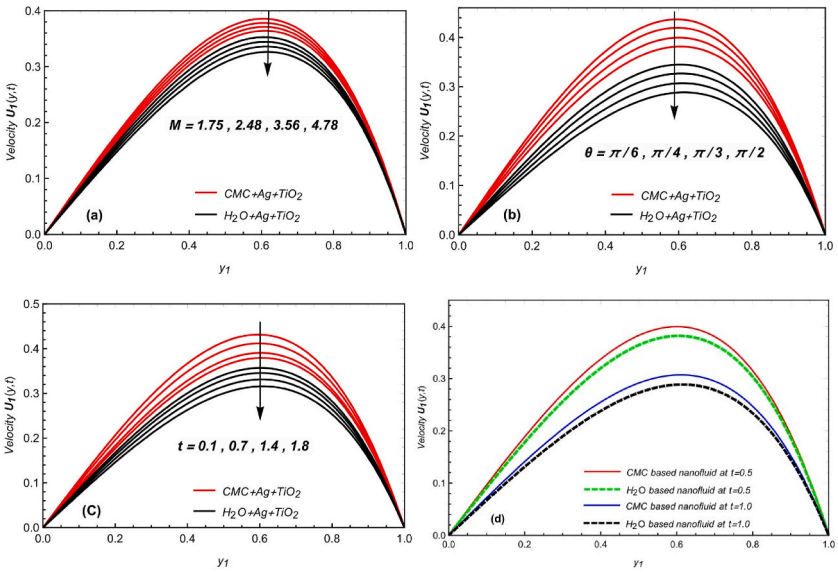

Fig. 5. $U_1(y,t)$ due to the influence of **(a):** M **(b):** θ **(c):** t **(d):** *Comparson of nanofluids* with $\alpha = \beta = 0.5, \varphi = 0.02, Gr = 8.5, Pr_{eff} = 6.3, Gm = 7.5, Sc = 2.5, \lambda_1 = 1.5$.

physical impact of fractional constraints on the flowing hybrid nanofluid flow mixed with $(Ag - TiO_2)$ nanoparticles and different base fluids. The velocity decreases when α, β are increased. Due to the rotational friction force and due to the kernel of the Fractal fractional of memory effect, the rotation parameter physically reduces the fluid's linear velocity, and the improvement in the memory effect also controls the fluid movement. While the fluid is spinning and flowing, flow is the result. In order to analyze the effect of *Gr and Gm* on the velocity profile, Fig. 3(c and d) are displayed. It is detected that the velocity profile increases by growing the value of heat grashof number and mass Grashof number. Physically, the momentum equation, which in this study contains the buoyancy component, is nondimensionalized to generate a nondimensional quantity called the Grashof number (*Gr*). *Gr* measures the ratio of buoyancy forces to viscous forces; hence, as *Gr* values rise, buoyancy forces rise while viscous forces reduce, increasing the flow velocity. Fig. 4(a–d) are plotted to study the impact of $pr_{eff}, Sc, \varnothing, \lambda_1$ on the velocity profile. It is observed that the velocity profile decreases while increasing the Prandtl number and Schmidt number, volume frictional, and Casson parameters, respectively. Physically, the velocity boundary layer will be thicker than the thermal boundary layer when the Prandtl number has increased. Thus, the Prandtl number has a very high physical relevance since it is the sole necessary dimensionless quantity that connects the thickness of the temperature and momentum boundary layers. Similarly, with the enhancement of other physical constraints, the fluid velocity is controlled and decreases asymptotically. Furthermore, for all considered constraints, the impact of (*CMC*) based hybrid nanofluid is much greater than the

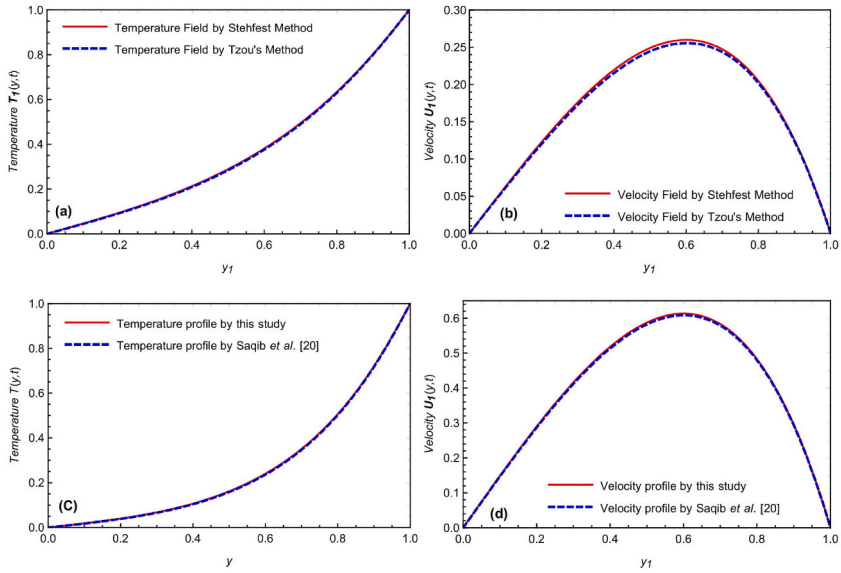

Fig. 6. Graphical validation of attained results by numerical results and Saqib et al. [20].

(H_2O)-based hybrid nanofluid like other constraints.

Fig. 5(a and b) illustrate how the applied magnetic field and the magnetic field's inclination, M, affect the momentum profile (a, b). The magnetic parameter M represents the Lorentz force, an antagonistic force that regulates the velocities of electrically conducting fluids. As M increases, the velocity decreases as a result. Physically, the large amount of M proves this is true since it strengthens the Lorentz forces, which seek to slow down motion. The graphs also display the straight-angle location of the greatest magnetic field strength. To examine the effects of time variation and to graphically compare various based fluids mixed with various regarded nanoparticles at various time values, Fig. 5(c and d) are shown. This demonstrates how the velocity impact can be managed over time. On the other side, the momentum profile decreases as time changes. Additionally, it can be shown in Fig. 5(d) that the momentum profile for the (CMC) base hybrid nanofluid is slightly higher than the water-based hybrid nanofluid, which decreases with the tightening of the time constraint because of the physical properties of the taken-into-account nanoparticles.

Using several numerical approaches and the results obtained by Saqib et al. [20], Fig. 6(a–d) are shown to validate the guided equation solutions we obtained. The mathematical solutions of all regulated equations are validated and satisfied by overlapping all curves. Comparisons of the concentration, temperature distributions, and velocity profiles between the results and those of Stehfest and Tzou are shown in Table 3. It is obvious that as y is increased, temperature distributions, concentration, and velocity all rise. These tables also show that our solutions satisfy the requirements for beginning and boundary. The numerical outcomes of the dimensionless Nusslet and Sherwood numbers for various nanoparticle forms are presented in Table 4. Contrary to declining nusslet and Sherwood numbers, the fractional parameter shows increasing values. The surface productivity of heat and mass convection is measured using the Nusselt and Sherwood values. Where the Nusselt number is to the thermal boundary layer, the Sherwood number is to the concentration boundary layer. Instead of forced convection, spontaneous convection is what causes the Sherwood number in this situation.

6. Conclusions

Through two parallel poured plates, the free convective flow of an unsteady, inviscid Casson-type flow mixed with a hybrid (Ag, TiO_2) nanofluid is examined with carboxymethyl cellulose (CMC) and water (H_2O) as base fluids. The most recent and better definition of a fractional derivative, known as a fractal fractional derivative, is used to generate a fractional model using the fractal Laplace transformation. Finally, the implications of various limitations on the collected energy, concentration, and momentum profile data are examined using graphical and numerical analysis. Here are some of the investigation's conclusive findings in bullet form:

- This strategy might be broadened to encompass a broader range of physical sciences categories with complex geometries.
- The heating and momentum profiles are both slowed down by Pr_{eff} enhancing value.
- The Schmidt number and fractional limitations are raised, which also decreases the rate o the concentration profile.
- The parameters Gr, Gm improve the momentum profile, whereas M and λ_1 declarations the momentum field.
- The fractional parameter can be used to modify both the momentum and the thermal boundary layer thickness.
- The found solutions can be used to test possible approximations of the solutions as needed and can help in accurately understanding the actual results.
- The findings of this inquiry are confirmed by the findings of Saqib et al. [20] and the flipping of both curves from the numerical solution.

Author statement

Kehong Zheng: Conceptualization, Methodology. Ali Raza: Data curation, Methodology, Writing- Original draft preparation. Ahmed M. Abed: Conceptualization, Data curation. Hina Khursheed: Data curation, Writing- Original draft preparation. Laila F. Seddek: Resources. Writing- Reviewing and Editing. Ali Hasan Ali: Software, Visualisation, Supervision, Writing- Reviewing and Editing. Absar Ul Haq: Investigation, Resources.

Declaration of competing interest

The authors declare that they have no known competing financial interests or personal relationships that could have appeared to influence the work reported in this paper.

Data availability

Data will be made available on request.

Acknowledgment

This study is supported via funding from prince Sattam bin Abdulaziz University project number (PSAU/R1/1444).

References

[1] F. Ali, M. Saqib, I. Khan, N. Ahmad Sheikh, Application of Caputo-Fabrizio derivatives to MHD free convection flow of generalized Walters'-B fluid model, Eur. Phys. J. Plus 131 (10) (2016) 377.
[2] F. Ali, N.A. Sheikh, I. Khan, M. Saqib, Solutions with Wright function for time fractional free convection flow of Casson fluid, Arabian J. Sci. Eng. 42 (2017) 2565–2572.
[3] A. Raza, et al., Numerical and computational analysis of magnetohydrodynamics over an inclined plate induced by nanofluid with Newtonian heating via fractional approach, Symmetry 14 (11) (2022) 2412.
[4] A. Raza, I. Khan, S. Farid, C.A. My, A. Khan, H. Alotaibi, Non-singular fractional approach for natural convection nanofluid with Damped thermal analysis and radiation, Case Stud. Therm. Eng. 28 (2021), 101373.
[5] M. Caputo, Linear models of dissipation whose Q is almost frequency independent, Ann. Geophys. 19 (4) (1966) 383–393.
[6] J. Singh, Analysis of fractional blood alcohol model with composite fractional derivative, Chaos, Solit. Fractals 140 (2020), 110127.
[7] W. Gao, B. Ghanbari, H.M. Baskonus, New numerical simulations for some real world problems with Atangana–Baleanu fractional derivative, Chaos, Solit. Fractals 128 (2019) 34–43.
[8] D. Kumar, J. Singh, D. Baleanu, On the analysis of vibration equation involving a fractional derivative with Mittag-Leffler law, Math. Methods Appl. Sci. 43 (1) (2020) 443–457.
[9] N.A. Sheikh, F. Ali, M. Saqib, I. Khan, S.A.A. Jan, A comparative study of Atangana-Baleanu and Caputo-Fabrizio fractional derivatives to the convective flow of a generalized Casson fluid, Eur. Phys. J. Plus 132 (2017) 1–14.
[10] F. Wang, et al., Heat and mass transfer of Ag− H2O nano-thin film flowing over a porous medium: a modified Buongiorno's model, Chin. J. Phys. (2023). https://doi.org/10.1016/j.cjph.2023.01.001.
[11] F. Wang, M.I. Asjad, M. Zahid, A. Iqbal, H. Ahmad, M. Alsulami, Unsteady thermal transport flow of Casson nanofluids with generalized Mittag–Leffler kernel of Prabhakar's type, J. Mater. Res. Technol. 14 (2021) 1292–1300.
[12] S.U. Choi, J.A. Eastman, Enhancing Thermal Conductivity of Fluids with Nanoparticles, Argonne National Lab.(ANL), Argonne, IL (United States), 1995.
[13] F. Wang, E. Hou, S.A. Salama, M.M. Khater, Numerical investigation of the nonlinear fractional Ostrovsky equation, Fractals 30 (5) (2022) 1–9.
[14] Z. Han, B. Yang, S.H. Kim, M.R. Zachariah, Application of hybrid sphere/carbon nanotube particles in nanofluids, Nanotechnology 18 (10) (2007), 105701.
[15] M.J. Nine, B. Munkhbayar, M.S. Rahman, H. Chung, H. Jeong, Highly productive synthesis process of well dispersed Cu2O and Cu/Cu2O nanoparticles and its thermal characterization, Mater. Chem. Phys. 141 (2–3) (2013) 636–642.
[16] J. Sarkar, P. Ghosh, A. Adil, A review on hybrid nanofluids: recent research, development and applications, Renew. Sustain. Energy Rev. 43 (2015) 164–177.
[17] J. Gómez-Aguilar, H. Yépez-Martínez, R. Escobar-Jiménez, C. Astorga-Zaragoza, L. Morales-Mendoza, M. González-Lee, Universal character of the fractional space-time electromagnetic waves in dielectric media, J. Electromagn. Waves Appl. 29 (6) (2015) 727–740.
[18] J. Singh, D. Kumar, Z. Hammouch, A. Atangana, A fractional epidemiological model for computer viruses pertaining to a new fractional derivative, Appl. Math. Comput. 316 (2018) 504–515.
[19] A. Atangana, K.M. Owolabi, New numerical approach for fractional differential equations, Math. Model Nat. Phenom. 13 (1) (2018) 3.
[20] M. Saqib, I. Khan, S. Shafie, New direction of Atangana–Baleanu fractional derivative with Mittag-Leffler kernel for non-Newtonian channel flow, Fractional Derivat. Mittag-Leffler Kernel: Trend. Appl. Sci. Eng. (2019) 253–268.
[21] A. Atangana, J. Gómez-Aguilar, Numerical approximation of Riemann-Liouville definition of fractional derivative: from Riemann-Liouville to Atangana-Baleanu, Numer. Methods Part. Differ. Equ. 34 (5) (2018) 1502–1523.
[22] T. Bakkyaraj, R. Sahadevan, Invariant analysis of nonlinear fractional ordinary differential equations with Riemann–Liouville fractional derivative, Nonlinear Dynam. 80 (2015) 447–455.
[23] A. Atangana, Fractal-fractional differentiation and integration: connecting fractal calculus and fractional calculus to predict complex system, Chaos, Solit. Fractals 102 (2017) 396–406.
[24] A. Atangana, M.A. Khan, Validity of fractal derivative to capturing chaotic attractors, Chaos, Solit. Fractals 126 (2019) 50–59.
[25] M. Imran, Application of fractal fractional derivative of power law kernel (FFP0Dxα, β) to MHD viscous fluid flow between two plates, Chaos, Solit. Fractals 134 (2020), 109691.
[26] Q. Haidong, et al., Analysis of non-equilibrium 4D dynamical system with fractal fractional Mittag–Leffler kernel, Eng. Sci. Technol. Int. J. 37 (2023), 101319.
[27] H.M. Srivastava, M. Izadi, Generalized shifted airfoil polynomials of the second kind to solve a class of singular electrohydrodynamic fluid model of fractional order, Fractal and Fractional 7 (1) (2023) 94.
[28] A.U. Rehman, M.B. Riaz, I. Khan, A. Mohamed, Time fractional analysis of Casson fluid with application of novel hybrid fractional derivative operator, AIMS Mathematics 8 (4) (2023) 8185–8209.
[29] K. Ramesh, M. Devakar, Some analytical solutions for flows of Casson fluid with slip boundary conditions, Ain Shams Eng. J. 6 (3) (2015) 967–975.
[30] A. Shloof, N. Senu, A. Ahmadian, M. Nouh, S. Salahshour, A novel fractal-fractional analysis of the stellar helium burning network using extended operational matrix method, Phys. Scripta 98 (3) (2023), 034004.
[31] K.A. Abro, Role of fractal–fractional derivative on ferromagnetic fluid via fractal Laplace transform: a first problem via fractal–fractional differential operator, Eur. J. Mech. B Fluid 85 (2021) 76–81.

[32] Z. Ali, F. Rabiei, K. Shah, T. Khodadadi, Modeling and analysis of novel COVID-19 under fractal-fractional derivative with case study of Malaysia, Fractals 29 (1) (2021), 2150020.
[33] Y.H. Youssri, A.G. Atta, Spectral collocation approach via normalized shifted Jacobi polynomials for the nonlinear lane-Emden equation with fractal-fractional derivative, Fractal and Fractional 7 (2) (2023) 133.
[34] S. Uçar, Analysis of hepatitis B disease with fractal–fractional Caputo derivative using real data from Turkey, J. Comput. Appl. Math. 419 (2023), 114692.
[35] A. Raza, K. Al-Khaled, T. Muhammad, S.U. Khan, Accelerating flow of carbon nanotubes with carboxymethyl cellulose and blood base materials with comparative thermal features: Prabhakar fractional model, Math. Probl Eng. 2023 (2023).
[36] A. Raza, M.Y. Almusawa, Q. Ali, A.U. Haq, K. Al-Khaled, I.E. Sarris, Solution of water and sodium alginate-based Casson type hybrid nanofluid with slip and sinusoidal heat conditions: a Prabhakar fractional derivative approach, Symmetry 14 (12) (2022) 2658.
[37] P. Mayeli, G.J. Sheard, Buoyancy-driven flows beyond the Boussinesq approximation: a brief review, Int. Commun. Heat Mass Tran. 125 (2021), 105316.
[38] Y.M. Chu, S. Bilal, M.R. Hajizadeh, Hybrid ferrofluid along with MWCNT for augmentation of thermal behavior of fluid during natural convection in a cavity, Math. Methods Appl. Sci. (2020). https://doi.org/10.1002/mma.6937.
[39] A. Raza, et al., Fractional order simulations for the thermal determination of graphene oxide (GO) and molybdenum disulphide (MoS2) nanoparticles with slip effects, Case Stud. Therm. Eng. 28 (2021), 101453.
[40] B. Guo, et al., Fractional-order simulations for heat and mass transfer analysis confined by elliptic inclined plate with slip effects: a comparative fractional analysis, Case Stud. Therm. Eng. 28 (2021), 101359.